RESEARCH ARTICLE SUMMARY

ENERGY STORAGE

Molecular solar thermal energy storage in Dewar pyrimidone beyond 1.6 megajoules per kilogram

Han P. Q. Nguyen, Alexander J. Maertens, Benjamin A. Baker, Nathan M.-W. Wu, Zihao Ye, Qingyang Zhou, Qianfeng Qiu, Navneet Kaur, David B. Berkinsky, Katherine E. Shulenberger, K. N. Houk*, Grace G. D. Han*

Full article and list of author affiliations: https://doi.org/10.1126/science.aec6413

INTRODUCTION: Heating accounts for nearly half of global energy consumption. However, nearly two-thirds of heating still relies on fossil fuels, such as natural gas, oil, and coal. As a result, heating is a major direct source of carbon emissions. Achieving a sustainable energy future, therefore, requires not only carbon-free electricity generation but also effective strategies for storing and delivering clean heat.

Molecular photoswitches have recently emerged as media for renewable solar energy storage and release. This concept is known as molecular solar thermal (MOST) energy storage. In MOST systems, photon energy is stored in the strained chemical bonds of a metastable photoisomer. Upon activation by an external stimulus, the metastable photoisomer reverts to its thermodynamically stable form, releasing the stored energy as heat ($\Delta H_{storage}$).

In this work, we report a MOST system based on 2-pyrimidone and its Dewar isomer, engineered for solvent-free operation and water compatibility. The system delivers a record-high gravimetric energy density under both neat and dilute aqueous conditions, enabling heat release and transfer sufficient to raise water to its boiling point under ambient conditions.

RATIONALE: Inspired by the aza-bicyclic framework of DNA lesions, we designed Dewar isomers that fuse highly strained 1,2-dihydroazete and diazetidine units to enhance the ring strain. We also incorporated a nitrogen atom at the reaction site, enabling labile C–N bond formation and cleavage. We hypothesized that combining high ring strain with a high-energy C–N bond would increase the energy of the metastable Dewar isomer, maximizing $\Delta H_{storage}$ and enabling controlled thermal release.

RESULTS: Pyrimidone derivatives were designed and synthesized with different alkylation patterns. This approach promoted efficient valence isomerization while maintaining low molecular weight. Upon excitation at 300 nm, pyrimidones underwent valence isomerization to form the corresponding Dewar isomers.

Differential scanning calorimetry showed that the Dewar isomers released exceptionally high $\Delta H_{storage}$ on thermal activation. The Dewar isomer reached a record-high gravimetric energy density of 1.65 MJ kg^{-1} (227.6 kJ mol^{-1}), exceeding values reported for leading MOST photoswitches. To demonstrate practical heat release and transfer, Dewar pyrimidone was dissolved in water, and an acid catalyst was used to promote the back isomerization. Addition of hydrochloric acid (HCl) to Dewar pyrimidone (107 mg in 0.46 ml of water) increased the solution temperature to 100°C and induced boiling within 1 s, demonstrating rapid macroscopic heat transfer to an environmentally benign medium under ambient conditions.

CONCLUSION: We developed a pyrimidone-based MOST system guided by two central design principles: (i) leveraging a highly strained, dearomatized aza-bicyclic scaffold to maximize stored energy and (ii) incorporating nitrogen at the reactive site to enable controllable thermal release. Together, these features yield a compact molecular architecture with an energy density of 1.65 MJ kg^{-1}. As a proof of concept, we demonstrated that heat output sufficient to boil 0.46 ml (460 mg) of water could be generated using 107 mg of Dewar pyrimidone. This result highlights the potential of MOST technology as a practical route toward scalable, on-demand heat delivery for water heating, cooking, and surface defrosting. □

*Corresponding author. Email: grace_han@ucsb.edu (G.G.D.H.); houk@ucla.edu (K.N.H.)
Cite this article as H. P. Q. Nguyen *et al.*, *Science* **392**, eaec6413 (2026). DOI: 10.1126/science.aec6413

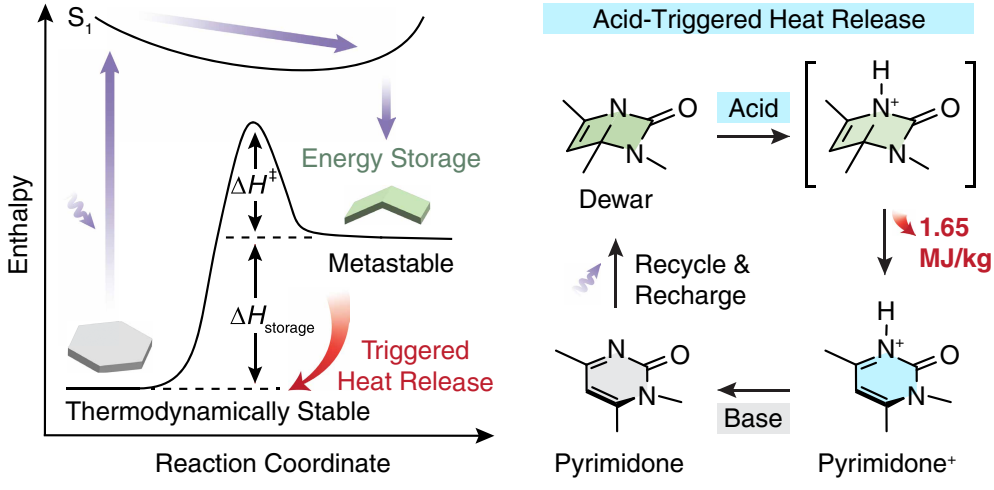

MOST energy storage in pyrimidone–Dewar pyrimidone. Energy diagram showcasing the photon energy storage and heat release through reversible Dewar isomerization (left). $\Delta H_{storage}$, energy storage density; $\Delta H^{\ddagger}$, enthalpy of activation. Acid-triggered reversion of the Dewar isomer enables rapid heat release, and the protonated pyrimidone is neutralized for recharging (right).

ENERGY STORAGE

Molecular solar thermal energy storage in Dewar pyrimidone beyond 1.6 megajoules per kilogram

Han P. Q. Nguyen[1,2], Alexander J. Maertens[3], Benjamin A. Baker[1,2], Nathan M.-W. Wu[2], Zihao Ye[3], Qingyang Zhou[3], Qianfeng Qiu[2], Navneet Kaur[2], David B. Berkinsky[2], Katherine E. Shulenberger[2], K. N. Houk[3]*, Grace G. D. Han[1,2]*

Storing sunlight in a compact and rechargeable form remains a central challenge for solar energy utilization. Molecular solar thermal (MOST) energy storage systems, which harness photon energy and release it as heat on demand, provide a direct approach but have long failed to meet practical benchmarks. Inspired by the architecture of DNA, we report a pyrimidone-based MOST system that stores energy in the strained Dewar photoisomer upon excitation at 300 nanometers. Designed with sustainability in mind, the system operates solvent free and remains compatible with aqueous environments while overcoming one of the field's greatest hurdles—the controlled extraction and transfer of stored heat. When catalyzed by acid, the Dewar isomer releases enough heat to boil water (~0.5 milliliters). These advances help point the way toward decentralized solar heat storage and off-grid energy solutions.

Heating accounts for nearly half of the global energy demand (*1*). Keeping homes warm in winter, providing hot water for daily use, and cooking meals are essential energy services that depend heavily on reliable heat supply. Yet almost two-thirds of this heating energy still comes from fossil fuels, such as natural gas, oil, and coal, which makes heating one of the largest direct sources of carbon emissions (*2*). The transition to a sustainable energy future therefore requires not only carbon-free electricity generation but also clean and storable heat.

Conventional off-grid heating relies on liquid fuels, such as heating oil, which can be easily stored and transported while presenting high combustion energy densities (40 MJ kg^{-1}) (*3*). In renewable systems, lithium-ion batteries are widely used for energy storage, with an effective energy density of 0.9 MJ kg^{-1} (*4*). When paired with solar panels, home battery systems can store electricity and power electric heaters, stoves, or boilers through Joule heating, in which electrical energy is directly converted into heat (*5*), enabling renewable thermal energy storage and release.

Recent advances in molecular photoswitches have opened up opportunities across a wide range of fields. These materials can reversibly transform between two or more distinct states under light, enabling applications in soft robotics (*6*), switchable catalysis (*7*), CO_2 capture (*8*), temperature sensing (*9*, *10*), protein modulation (*11*), and mechanically interlocked molecule synthesis (*12*).

Beyond these functions, molecular photoswitches have recently emerged as media for renewable solar energy storage and release—a concept known as molecular solar thermal (MOST) energy storage. In these systems, photon energy is captured and stored in the strained chemical bonds of a metastable photoisomer, which can later be triggered to revert to its thermodynamically stable form, releasing heat. Representative MOST systems include the photoisomerizing azo(hetero)arenes (*13*, *14*), hydrazones (*15*), dihydroazulenes (*16*, *17*), fulvalene diruthenium (*18*–*20*), norbornadienes (*21*–*28*), bicyclooctadienes (*29*), azaborinines (*30*, *31*), and curved anthracenes (*32*).

The performance of a MOST compound is determined by several key parameters, which include enhanced light absorption (*33*–*36*), robust resistance to fatigue (*37*–*40*), efficient isomerization with high quantum yield (*41*–*43*), tunable activation energy for reversion to the thermodynamically stable state ($\Delta H^{\ddagger}$) (*44*–*46*), and large energy storage density ($\Delta H_{storage}$) (*31*, *32*)—i.e., the energy difference between the stable and metastable states. The latter two properties are particularly crucial because a sufficiently high $\Delta H^{\ddagger}$ enables long-term energy retention (*47*, *48*), whereas the historically low $\Delta H_{storage}$ has limited the translation of the MOST concept into practical heating applications (*49*, *50*). To maximize $\Delta H_{storage}$, it is advantageous to focus on small molecules that undergo photoisomerization to highly strained metastable isomers (*51*).

Photoinduced valence isomerization, a pericyclic reaction occurring in some small molecules, has been demonstrated in MOST systems. For instance, norbornadiene undergoes an intramolecular [2+2] photocycloaddition to form quadricyclane, thereby storing energy in a strained cyclic structure (*26*). This system exhibits one of the highest gravimetric energy storage densities of 0.97 MJ kg^{-1} (89 kJ mol^{-1}) among all MOST compounds. Another type of valence isomerization—i.e., Dewar isomerization, which involves photoinduced loss of aromaticity—holds promise for maximizing $\Delta H_{storage}$. Recently, azaborinines and their Dewar isomers were reported as an emerging MOST system with gravimetric energy densities of up to 0.65 MJ kg^{-1} (201 kJ mol^{-1}) per active monomeric unit (*30*, *31*). The notably high molar energy density of this system could be due to the loss of aromaticity upon isomerization, which increases the energy gap between the stable aromatic isomer and the metastable nonaromatic isomer (*52*–*54*).

However, the absorption of norbornadienes is restricted to the ultraviolet C (UV-C) range (<280 nm), requiring artificial light sources (*55*) for energy storage. Although functionalization strategies have red shifted their absorption profile to harness the solar spectrum more, they also increase molecular weight, thereby reducing gravimetric energy densities to 0.10 to 0.73 MJ kg^{-1} (*22*–*24*). Similarly, azaborinines offer higher molar energy densities but require bulky substituents to prevent side reactions, such as polymerization, which again compromises gravimetric energy densities (*31*). Furthermore, like many MOST systems reported to date, both norbornadiene and azaborinine operate in solution (*56*, *57*), which substantially lowers their effective gravimetric and volumetric energy densities for fuel applications. Finally, other areas of material research have demonstrated successful incorporation of water-compatible designs (*58*–*61*). By contrast, the general incompatibility of MOST systems with aqueous environments restricts their integration into water-based or environmentally sustainable heating applications.

As a result, there is a critical need for MOST systems that offer high energy density, function under solvent-free conditions (*62*), and incorporate sustainable features such as compatibility with aqueous environments. To address this, we looked to nature for inspiration. A fascinating photochemical process in DNA suggests a new direction for photochemical fuel development. When exposed to high-energy UV light (UV-B or UV-C), nucleobases in DNA can form a derivative of 2-pyrimidone called a (6-4) lesion (*63*). Further irradiation with lower-energy UV input (UV-A or UV-B) induces the formation of the Dewar isomer. These Dewar lesions are thought to disrupt DNA replication, causing mutations that may lead to cancer (*64*, *65*). Evolution has led to the development of (6-4) photolyase, an enzyme capable of converting the Dewar isomer back into the thermodynamically

[1]Department of Chemistry and Biochemistry, University of California, Santa Barbara, CA, USA. [2]Department of Chemistry, Brandeis University, Waltham, MA, USA. [3]Department of Chemistry and Biochemistry, University of California, Los Angeles, CA, USA. ***Corresponding author. Email: grace_han@ucsb.edu (G.G.D.H.); houk@ucla.edu (K.N.H.)**

stable 2-pyrimidone (*63*). Inspired by this reversible Dewar valence isomerization reaction, we became interested in the potential of 2-pyrimidone as a MOST system along with two related scaffolds, 2-pyridone and 4-pyrimidone.

Derivatives of 2-pyridone and 4-pyrimidone can undergo both forward and reverse Dewar isomerization, but low conversion makes them suboptimal candidates for MOST systems. For example, irreversible [4+4] intermolecular dimerization of 2-pyridone suppresses Dewar formation (*66*, *67*). Dewar isomers of 4-pyrimidones fail to revert quantitatively because of side reactions during thermal activation (*68*, *69*). By contrast, 2-pyrimidone has demonstrated both quantitative photoinduced isomerization and thermally induced reversion (*70*), which makes it a more promising scaffold.

In this study, we report a MOST system based on 2-pyrimidone and its Dewar isomer, engineered for both solvent-free operation and water compatibility. By systematically tuning substituents at the 1-, 4-, and 6-positions of the aromatic core, we optimized energy storage performance while maintaining reversible switching behavior. Notably, our system demonstrates a record-high gravimetric energy density under neat and dilute aqueous conditions, enabling thermal release at a level sufficient to bring water to its boiling point under ambient conditions.

Molecular design

Pyrimidones **1** to **4** (50 mg, 4 to 20 mM) in acetonitrile (ACN) were irradiated in a photoreactor equipped with commercially available 300-nm lamps. After 24 hours, the formation of the corresponding Dewar isomers was observed. The Dewar isomers were isolated and characterized by ^{1}H and ^{13}C nuclear magnetic resonance (NMR) spectroscopy (figs. S1 to S8), which showed upfield shifts consistent with loss of aromaticity, in agreement with previous studies of pyrimidone valence isomerization (*70*, *71*). We discovered that the Dewar isomers in neat liquid states reverted to their pyrimidone forms when heated above 170°C, confirming the reversibility of the photo-thermal cycle (vide infra).

This reversible photoisomerization behavior establishes the pyrimidone-Dewar pair as a viable MOST system. In this system, pyrimidone (P) undergoes valence isomerization to form Dewar (D) isomers, which can be thermally activated to revert to their thermodynamically stable pyrimidone forms, releasing stored energy ($\Delta H_{storage}$) (Fig. 1A). Inspired by the distinct aza-bicyclic architecture of DNA lesions, these Dewar isomers fuse highly strained 1,2-dihydroazete (*72*, *73*) and diazetidine (*74*) units, resulting in a compounded strain (*75*). We also strategically incorporated a nitrogen atom at the reaction site, enabling labile C–N bond formation and cleavage (*47*). We hypothesized that this combination of compounded strain and high-energy C–N bond in the Dewar isomer would increase the energy of the metastable state, enhancing $\Delta H_{storage}$ and efficiently controlling thermal release.

To maximize gravimetric energy density, we prioritized lightweight, compact molecular design. Because tautomerization (i.e., keto and enol) competes with the desired photochemical pathway (*76*), the sp^3 secondary nitrogen was methylated to suppress this process. However, attempts to isomerize 1-methyl-2-pyrimidone were unsuccessful, yielding no detectable Dewar isomers using NMR spectroscopy, which was rationalized computationally (vide infra). Therefore, to promote efficient valence isomerization while maintaining a low molecular weight (<138 g mol^{-1}), additional methyl substituents were introduced to the pyrimidone ring. Three methylated derivatives with distinct substitution patterns—1,4-dimethyl-2-pyrimidone (**1**), 1,6-dimethyl-2-pyrimidone (**2**), and 1,4,6-trimethyl-2-pyrimidone (**3**)—were synthesized (Fig. 1B). All three compounds can be obtained through one-step nucleophilic

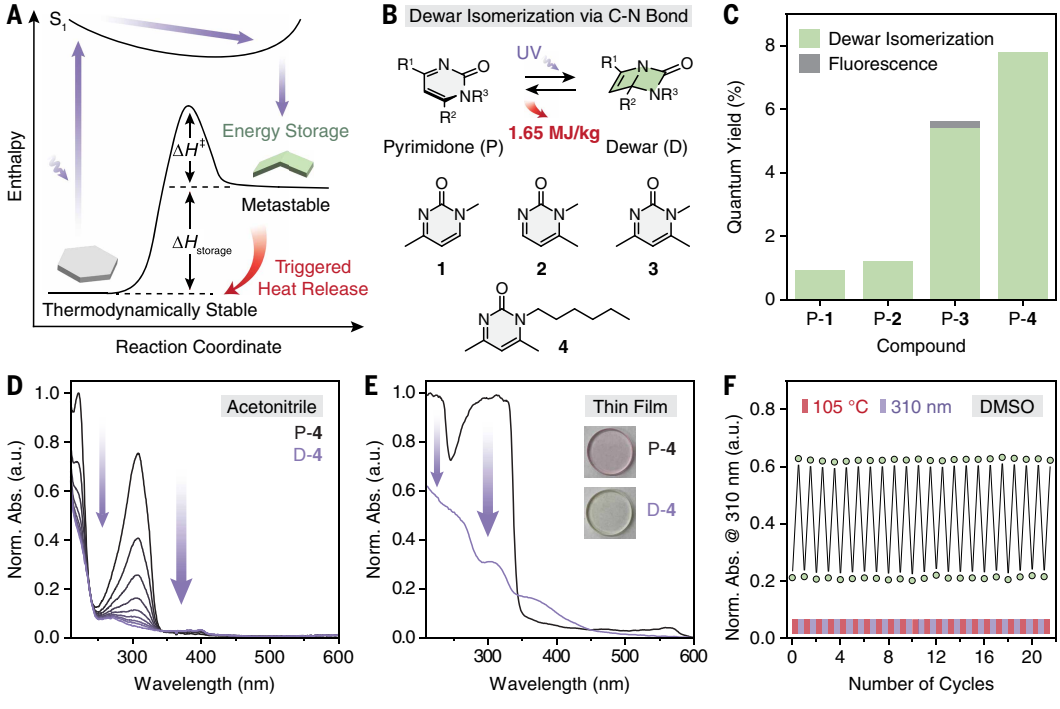

Fig. 1. Energy storage and release through reversible Dewar isomerization. (**A**) An energy diagram illustrating solar photon energy storage through Dewar isomerization and energy release by triggered electrocyclic ring opening. (**B**) Reversible photoinduced Dewar isomerization of pyrimidone derivatives **1** to **4** with varied alkylation patterns. (**C**) Dewar isomerization quantum yield of P-**1** to P-**4** and fluorescence quantum yield of P-**3** in ACN. (**D**) Normalized UV-Vis spectral changes upon the photoisomerization of P-**4** in ACN obtained from irradiation at 310 nm. a.u., arbitrary units. (**E**) Normalized thin-film UV-Vis absorption spectra of P-**4** and D-**4** obtained from irradiation at 310 nm. Insets display optical images of the thin film before and after irradiation corresponding to the UV-Vis spectra. (**F**) More than 20 cycles of reversible isomerization of D-**3** in DMSO induced by thermal treatment at 105°C and subsequent irradiation at 310 nm.

substitution or condensation from inexpensive, commercially available precursors. Compound ***3*** was synthesized on a multigram scale, which highlights its low cost and potential for commercial scalability.

Although the more compact structures of compounds **1** and **2** were initially expected to deliver superior energy storage performance, compound ***3*** exhibited the highest gravimetric energy storage capacity, establishing the 1,4,6-substitution pattern as optimal. Building on this insight, we designed a liquid-phase derivative, 4,6-dimethyl-1-hexyl-2-pyrimidone (**4**), tailored to undergo isomerization and thermal reversion under solvent-free conditions. All compounds were fully characterized by NMR spectroscopy and high-resolution mass spectrometry (figs. S9 to S16).

Light-induced isomerization of pyrimidones

Our computational mechanistic investigation of the natural orbitals obtained using extended multistate complete active space second-order perturbation theory (XMS-CASPT2) calculations of the ground state and Franck-Condon (FC) point suggests that the photochemical Dewar isomerization of pyrimidone is initiated by n–π* excitation to the S_1 excited state (figs. S17 and S18). The predicted excitation wavelength for P-***3*** (λ_{cal} = 311 nm) is in good agreement with the experimentally measured absorption maximum (λ_{max} = 307 nm) (fig. S19). When irradiated with a 300-nm or 310-nm lamp, the characteristic n–π* absorption band of P-***3*** decreased over time, indicating the formation of D-***3***, consistent with our NMR characterization. To assess photocharging efficiency, the photoisomerization quantum yields of P-**1** to P-**4** under 310-nm irradiation were measured in ACN and found to range from 0.9 to 7.8% (Fig. 1C, fig. S20, and table S1).

Excited-state [XMS-CASPT2 and density functional theory (DFT)] calculations indicate that the parent pyrimidone, 1-methyl-2-pyrimidone, exhibits a fast rate of intersystem crossing (ISC) from the S_1 n–π* surface to the T_1 π–π* excited state ($k_{ISC\ S1\rightarrow T1} \sim 10^{10}\ s^{-1}$), consistent with El-Sayed's rule (*77*), followed by rapid ($k_{ISC\ T1\rightarrow S0} \sim 10^{7}\ s^{-1}$) nonradiative decay back to the ground state (fig. S18). As a result, both fluorescence ($k_{FL} \sim 10^{6}\ s^{-1}$) and phosphorescence ($k_{phosp} \sim 10^{1}\ s^{-1}$) are disfavored. This suggests that the prominent nonradiative decay process, rather than photoluminescence, contributes to the low photoisomerization quantum yields. An experimentally measured photoluminescence quantum yield of 0.2% for P-***3*** (Fig. 1C and fig. S21) corroborates this theory.

At present, the pyrimidones that we have studied absorb primarily in the UV-A and UV-B region [~5% of the solar spectrum (*78*)] (Fig. 1D and fig. S19), and the relatively low photoisomerization quantum yields further contribute to the extended charging durations under solar irradiation. To investigate whether future modifications might improve the charging process, we have studied computationally whether substitutions can red shift the absorption of pyrimidone. Computations summarized in table S2 indicate that introducing a strong donor –NMe_2 at the 4-position or an electron-withdrawer or conjugator –CN and –Ph at the 4- and 6-positions, respectively, will induce a bathochromic shift. These substitutions result in a modest reduction in gravimetric energy density owing to the increased molecular weight. Exploration of such compounds in the future is planned.

Pyrimidones **1** to **4** and their Dewar isomers exhibit minimal spectral overlap in the n–π* absorption region (Fig. 1D), which enables high (90 to 93%) conversion in compounds **1** and **2** and quantitative conversion (100%) in compounds ***3*** and **4** under continuous irradiation in ACN (figs. S1 to S8). The results were consistent across multiple runs with less than 5% variation in conversion. Notably, liquid-state P-**4** also underwent effective isomerization under neat conditions (Fig. 1E), eliminating the need for solvent. However, we note that heat release under neat conditions can lead to self-heating (*50*) and potential thermal runaway. We therefore opted to conduct the thermal discharge of the Dewar isomer in organic or aqueous media to ensure controlled heat release. Detailed conditions for energy release in neat and solution states are illustrated in the next section.

To further underscore practicality, we demonstrated the long-term chemical and thermal stability of our pyrimidone over multiple energy storage and release cycles. We aim to create a MOST system capable of storing and releasing heat with total usable energy comparable to conventional heating oil for decentralized residential heating. Conventional heating oil provides heat through a linear, single-use process that involves (i) crude oil extraction, (ii) refining, (iii) distribution, and (iv) combustion (fig. S22A) (*79*, *80*). Each heating cycle consumes the fuel irreversibly, generating (v) greenhouse gas emissions. By contrast, a MOST system—e.g., pyrimidone-Dewar—operates in cycles (fig. S22B, steps ***3.1*** to ***3.3***). After initial synthesis and distribution to end users, pyrimidone can be charged by light to store energy in its metastable Dewar isomer. The stored energy is retained until heat is required, at which point activation releases the stored heat and regenerates the pyrimidone form. This charge-discharge process is reversible, allowing energy to be extracted multiple times from the same material until performance degradation ultimately necessitates its replacement. Given that the combustion energy of heating oil is ~40 MJ kg^{-1} (*3*), a MOST compound storing 1.5 to 2 MJ kg^{-1} per cycle and operating reversibly for at least 20 cycles could deliver a comparable cumulative thermal output at a similar mass. On this basis, compound ***3*** was selected for cyclability testing on account of its facile synthesis and representative energy-release performance (vide infra).

Charge-discharge cycling of compound ***3*** (5×10^{-5} M, 3 ml) was monitored by ultraviolet-visible (UV-Vis) spectroscopy (Fig. 1F). Photocharging was carried out by irradiation at 310 nm, whereas thermal discharge was activated by heating using a temperature-controlled cuvette holder with built-in stirring. To efficiently induce the thermal reversion [half-life ($t_{1/2}$) = 481 days at room temperature], the D-***3*** solution was heated to 105°C, the maximum operational temperature of our cuvette holder. As a result, dimethyl sulfoxide (DMSO) was selected to ensure chemical stability and avoid solvent loss during repeated heating (~75 min) and irradiating (~15 min) cycles. Under these conditions, the system showed negligible degradation over more than 20 photoisomerization–thermal reversion cycles in DMSO, confirming the robustness and reversibility.

Remarkable energy storage in Dewar pyrimidones

Pyrimidones exhibit different phase behavior depending on functionalization. Pyrimidones **1** to ***3*** are solids at room temperature, whereas pyrimidone **4** is intrinsically liquid per design (Fig. 2A and fig. S23). By contrast, the Dewar isomers generated by irradiating pyrimidones are all obtained as liquids, storing energy. Using differential scanning calorimetry (DSC), we observed and quantified the exothermic heat release ($\Delta H_{storage}$) associated with the D→P reversion in neat conditions. When heated at 10°C min^{-1} from room temperature to above 170°C, Dewar isomers undergo D→P electrocyclic ring opening, releasing the stored energy ($\Delta H_{storage}$) and generating molten pyrimidones at high temperatures. Pyrimidones ***3*** and **4** exhibit excellent thermal stability even at high temperatures, showing negligible thermal decomposition (fig. S24). The NMR spectra of restored pyrimidones after DSC are shown in figs. S25 to S32.

Notably, both molecular and gravimetric energy storage densities, measured as exotherms, reach values of 1.65 MJ kg^{-1} or 228 kJ mol^{-1} (Table 1). The storage capacities per mass of the pyrimidone system surpass those of leading photoswitches by at least 65%, including trimeric azaborinine [0.99 MJ kg^{-1} (*81*)], norbornadiene [0.97 MJ kg^{-1} (*26*)], and Dewar anthracene [0.65 MJ kg^{-1} (*32*)] (Fig. 2, B and C). The relevant thermal parameters for the electrocyclic ring-opening processes are summarized in Table 1, and additional physicochemical properties are provided in tables S3 and S4.

The observed outstanding performance of pyrimidones aligned with our hypothesis, confirming the effectiveness of our strategic molecular design. First, the Dewar structure was engineered to experience a

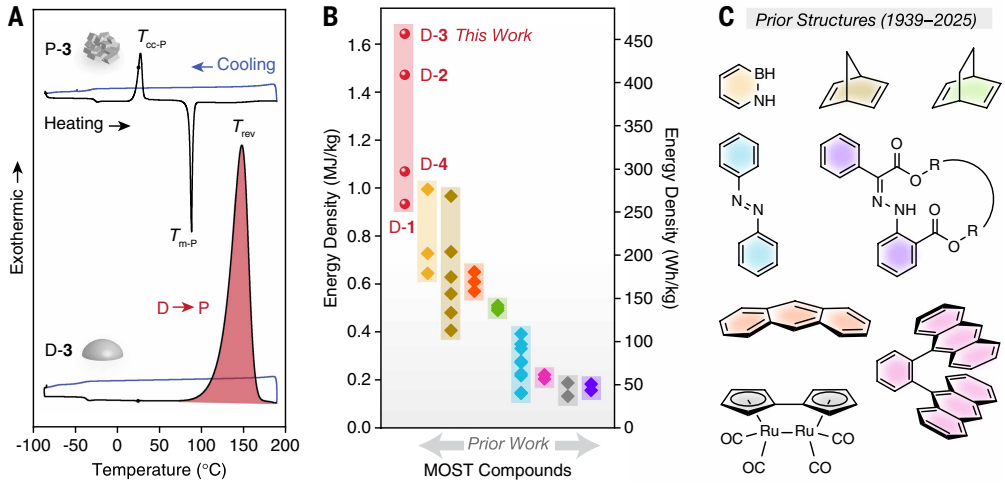

Fig. 2. Energy storage capacity of Dewar pyrimidones. (**A**) DSC thermograms of P-**3** and D-**3** measured during the first heating (black) and cooling (blue) cycle. Red highlighted area represents the exotherm of reversion ($\Delta H_{storage}$). T_{m-P}, melting point of pyrimidone; T_{cc-P}, cold crystallization point of pyrimidone; T_{rev}, peak thermal reversion temperature. The black dot on each plot marks the onset of data recording at ambient temperature. (**B**) Gravimetric energy densities of Dewar isomers **1** to **4** compared with prior MOST photoswitches. (**C**) Chemical structures of prior MOST compounds—i.e., (left to right, top to bottom) azaborinines (*30*,*31*,*81*), norbornadienes (*23*–*28*), bicyclooctadienes (*29*), azo(hetero)arenes (*95*–*103*), hydrazones (*15*), curved anthracenes (*32*), *ortho*-dianthrylbenzenes (*104*,*105*), and fulvalene dirutheniums (*19*,*20*).

Table 1. Thermal parameters for the retro-electrocyclization processes. T_{rev}, peak thermal reversion temperature; $\Delta H_{storage}$, energy storage density; $\Delta H^{\ddagger}$, enthalpy of activation; $t_{1/2}$, extrapolated half-life of Dewar isomer at 298 K; ΔH_{cal}, DFT-calculated energy storage density; $\Delta H^{\ddagger}_{cal}$, DFT-calculated enthalpy of activation; N/A, not applicable.

D→P	T_{rev} (°C)	$\Delta H_{storage}$ (kJ mol^{-1})	$\Delta H_{storage}$ (MJ kg^{-1})	$\Delta H^{\ddagger}$ (kJ mol^{-1})	$t_{1/2}$ (days)	ΔH_{cal} (kJ mol^{-1})	$\Delta H^{\ddagger}_{cal}$ (kJ mol^{-1})
1	176.3 ± 3.3	132.9 ± 1.2*	1.070 ± 0.009*	N/A§	N/A§	225	156
2	134.6 ± 0.5	183.2 ± 3.7†	1.476 ± 0.030†	100.0 ± 3.1	80	222	135
3	148.7 ± 0.5	227.6 ± 1.4	1.648 ± 0.010	113.1 ± 2.3	481	215	137
4	159.8 ± 0.1	194.7 ± 0.6	0.935 ± 0.003	115.6 ± 0.9	1240	225	152

*Estimated $\Delta H_{storage}$ of 100% D-**1** derived from experimentally obtained $\Delta H_{storage}$ of 93:7 D-**1**:P-**1** mixture. †Estimated $\Delta H_{storage}$ of 100% D-**2** derived from experimentally obtained $\Delta H_{storage}$ of 90:10 D-**2**:P-**2** mixture. §D-**1** did not exhibit a clean thermal reversion to P-**1** and instead underwent decomposition below 80°C in DMSO, preventing the determination of reliable kinetic parameters.

compounded strain within the fused bicyclic motif. Second, replacing the traditional C–C bond that is formed and cleaved in MOST systems with a more labile C–N bond enables substantially higher $\Delta H_{storage}$ compared with Dewar anthracene and azaborinine systems that store less than 201 kJ mol^{-1}. Finally, Dewar isomerization of pyrimidone also results in a complete loss of aromaticity, in contrast to systems such as Dewar anthracene, where aromaticity is only partially disrupted upon photoisomerization (*32*, *53*). Together, these features produce markedly strained and high-energy Dewar pyrimidones, reaching energy storage levels previously inaccessible to MOST systems.

Additionally, we experimentally determined the thermal activation energies ($\Delta H^{\ddagger}$) and extrapolated half-lives ($t_{1/2}$) for the electrocyclic ring opening of the Dewar isomers in DMSO (figs. S33 to S36 and table S5). The Dewar isomers **2** to **4** demonstrate outstanding thermal stability in solution, with $t_{1/2}$ values ranging from months to 3 years (Table 1), despite their high energy states compared with the parent pyrimidones. The long $t_{1/2}$ values highlight their strong potential for durable, long-term energy storage even under fluctuating temperature conditions. We note that the thermal reversion kinetics of D-**1** were not successfully obtained because of side reactions upon heating.

Mechanistic investigations

Our theoretical studies elucidate the photochemical and thermal reaction mechanism of the pyrimidone system (Fig. 3A). Quantum mechanical calculations suggest that Dewar isomerization of P-**3** proceeds through photon absorption, which initially excites the molecule to the FC n–π* singlet state (fig. S37), then rapidly relaxes to a minimum on the S_1 excited-state surface, the adiabatic point (Ad). This excited state advances to the conical intersection (CI) point, followed by fast decay to the ground state with accompanying heat evolution, forming D-**3**. Pyrimidones **1**, **2**, and **4** follow similar mechanistic pathways, with only minor differences in the energetic profiles (fig. S38). The parent pyrimidone, 1-methyl-2-pyrimidone, displays an energetically elevated FC point (405 kJ mol^{-1}), which potentially accounts for its unsuccessful Dewar isomerization.

Calculation of the 4π-electrocyclic ring-opening reaction coordinate of each pyrimidone highlights the influence of the methyl groups at the 4- and 6-positions on the thermal reversion kinetics of Dewar isomers. Compared with 1-methyl-2-pyrimidone ($\Delta H^{\ddagger}_{cal}$ = 150 kJ mol^{-1}), compounds **2** to **4** bearing a 6-methyl group exhibit a lower $\Delta H^{\ddagger}_{cal}$ (Table 1). Conversely, compound **1**, which features a 4-methyl substituent, displays a higher $\Delta H^{\ddagger}_{cal}$. Furthermore, computational studies on a series of theoretical analogs revealed these substitution effects to be consistent and additive (fig. S39). Our experimental measurements of $\Delta H^{\ddagger}$ and the reversion temperature (T_{rev}) in DSC showed excellent agreement with the theoretical predictions.

We sought to further explore the mechanism behind the observed methyl group substitution effect. Hirshfeld charge and spin analysis reveal that the 6-methyl substituent lowers the thermal reversion barrier by stabilizing the TS (Fig. 3B). Whereas the TS of 1-methyl-2-pyrimidone exhibits diradical character, that of P-**3** features δ^+ charge accumulation at C6 and zwitterionic character. The polarization of the highest occupied natural orbital (HONO) and the lowest unoccupied natural orbital (LUNO) stabilizes the TS, thereby lowering $\Delta H^{\ddagger}_{cal}$ (figs. S40 and S41) (*82*). Natural orbital analysis from multireference calculations [complete active space self-consistent field (CASSCF)] of the two transition states corroborates this observation (fig. S42). Stabilization energy analysis derived from an isodesmic reaction model confirms that the 6-methyl substituent stabilizes the TS more strongly than the Dewar isomer (Fig. 3C). The analysis also finds that the 4-methyl group stabilizes the Dewar isomer more than the TS, which in turn increases the $\Delta H^{\ddagger}_{cal}$. We hypothesize that the 4-methyl group contributes to D-**2** stabilization through hyperconjugation (*83*, *84*). The computational details are included in figs. S43 to S45 and table S6.

We then shifted focus to connect our understanding of the reaction thermodynamics to structural mechanistic features of the pyrimidone by constructing a univariate linear free energy relationship. We evaluated

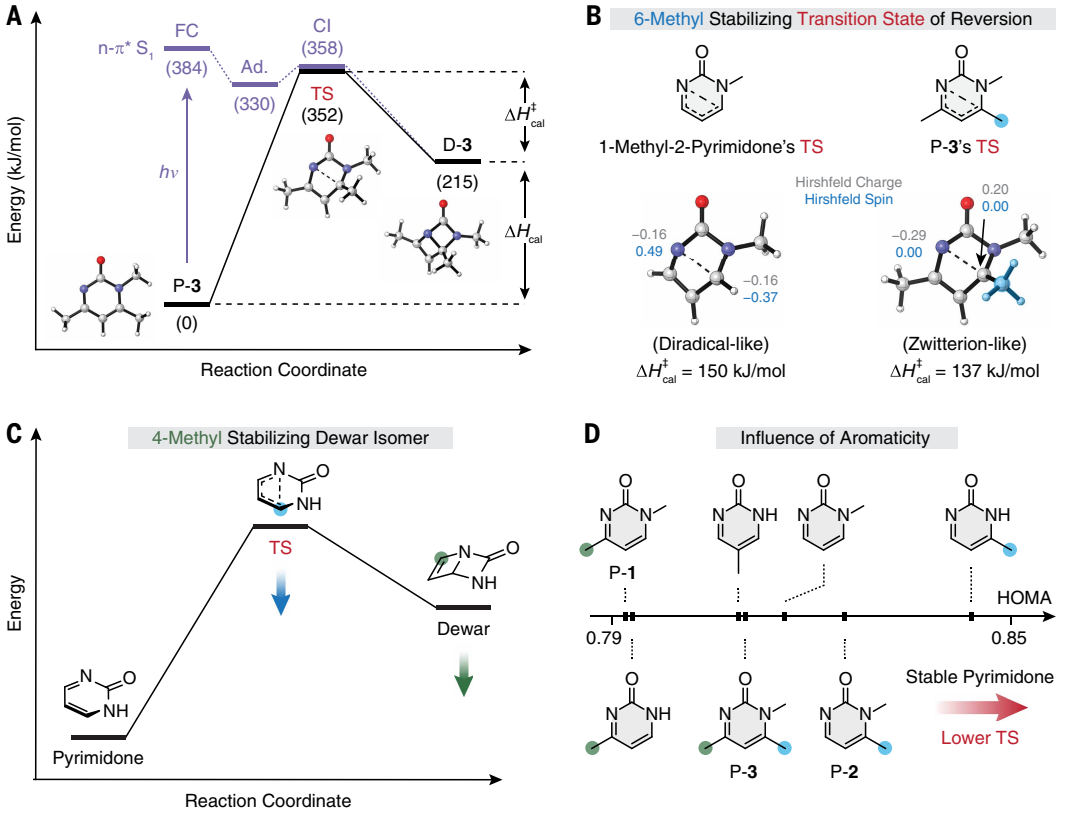

Fig. 3. DFT calculations of reversible Dewar isomerization process. (**A**) Photochemical Dewar isomerization mechanism of P-**3** (purple line) and thermal electrocyclic ring-opening mechanism of D-**3** (black line). (**B**) Hirshfeld charge and spin analysis of 1-methyl-2-pyrimidone and P-**3** in the transition state (TS) during the thermal reversion of their respective Dewar isomers. (**C**) Illustration of the stabilizing effect of a methyl substituent at the 4- and 6-positions on the Dewar 2-pyrimidone and the TS. (**D**) Correlation between HOMA of pyrimidone derivatives and their TS energy. ΔH_{cal}, calculated energy storage density; $\Delta H^{\ddagger}_{cal}$, calculated enthalpy of activation. All enthalpies were calculated using: (U)ωB97X-D/def2-TZVPP/PCM(DMF)//(U)ωB97X-D/def2-SVP/PCM(DMF) at 298.15 K and 1 atm. Excited-state electronic energies were calculated at XMS-CASPT2(10e,8o)/def2-TZVPP//XMS-CASPT2(10e,8o)/def-2-SVP.

the aromaticity of several pyrimidones using the harmonic oscillator model of aromaticity (HOMA) (Fig. 3D) (*85*, *86*). A clear correlation between increasing aromatic character (1-methyl-2-pyrimidone < P-**1** < P-**3** < P-**2**) and 4π-electrocyclic ring-opening activation energy was observed, indicating that progressive stabilization of the pyrimidone ring accelerates thermal reversion. According to the Bell–Evans–Polanyi principle (*87*–*89*), greater stabilization of the ground-state pyrimidone leads to a more stabilized TS, thereby lowering the activation barrier (i.e., $\Delta H^{\ddagger}$) to thermal reversion (fig. S46). Taken together, the interplay between aromaticity and the selective effects of the methyl substituents at the 4- and 6-positions explain the trend in both experimental and calculated $\Delta H^{\ddagger}$ values (Table 1).

Calculated energy storage density (ΔH_{cal}) values across the derivatives are generally high, exceeding 200 kJ mol^{-1} (fig. S39). These values are much greater than the experimental $\Delta H_{storage}$ for compounds **1**, **2**, and **4** but are comparable to that of compound **3** (Table 1). We propose that the thermal decomposition of compounds **1** and **2** (figs. S23 and S24) occurs in parallel with the thermally activated reversion pathway, thereby suppressing the overall heat release attainable from the system. The deviation observed in compounds **3** and **4** may be attributed to the different intermolecular interactions. Specifically, compound **4** contains a long hexyl chain, which introduces van der Waals interactions that may disrupt π–π stacking among the parent pyrimidones, thereby destabilizing it. As a result, compound **4** exhibits a lower $\Delta H_{storage}$ than compound **3**, both on a per-mole and per-mass basis.

Despite the lower $\Delta H_{storage}$, compound **4** was specifically tailored for solvent-free operation and a longer energy storage period (3 years versus 1 year). By contrast, compound **3**, with its compact structure and high thermal tolerance, delivers record-high energy density of 1.65 MJ kg^{-1} and 228 kJ mol^{-1}.

Heating water with Dewar pyrimidone

MOST systems offer a promising strategy for the controllable capture, storage, and release of solar energy. Over the years, this field has envisioned their integration into a scalable device with a closed-loop architecture (Fig. 4A) (*90*, *91*). In this concept, a MOST compound is dissolved in a circulating solvent that flows through a channel exposed to sunlight. As the solution passes through the illuminated region, the molecules convert from their thermodynamically stable form to a metastable, energy-rich isomer, thereby storing solar energy in chemical bonds. The charged solution is then collected in a reservoir, where the stored energy can be retained for later use. When needed, the solution is directed through a trigger module containing a catalyst embedded within the flow channel. The catalyst triggers the reversion of the metastable isomer to its thermodynamically stable form, releasing the stored energy as heat. This thermal energy is transferred through a heat exchanger to a heat-transfer fluid (e.g., cold water), enabling controlled and efficient heat extraction for practical use, such as space and water heating.

In this work, we present a simplified proof of concept showing direct heat release and transfer to a typical heat-transfer medium or water.

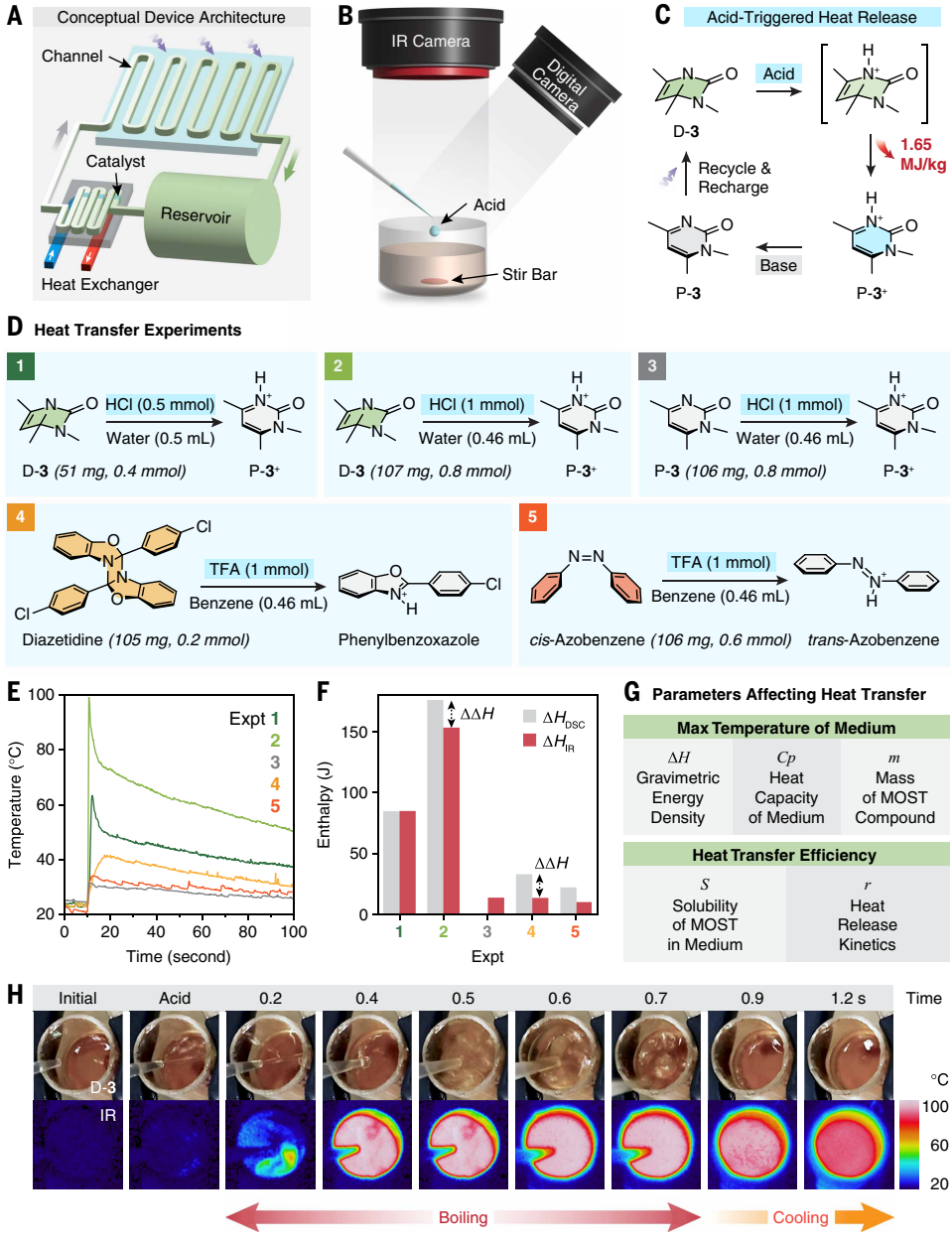

Fig. 4. Macroscopic heat release and transfer. (**A**) Schematic representation of a conceptual MOST energy storage and release device operating in a closed-loop configuration (*90*, *91*). (**B**) Schematic of the experimental setup. A custom-made cylindrical glass vessel (15 mm in diameter) was used to hold the stirred sample solution. Temperature changes were recorded using a high-resolution IR thermal imaging camera, and physical changes were captured with a digital camera positioned at a tilted angle. (**C**) Mechanism of acid-triggered thermal reversion of D-**3** to P-**3**. (**D**) Acid-triggered heat-transfer experiments **1** to **5** conducted on different substrates—i.e., D-**3**, P-**3**, diazetidine, and *cis*-azobenzene. (**E**) Temperature profiles from experiments **1** to **5**. Temperatures were extracted from the hottest pixel (hotspot) on the surface of the solution. (**F**) DSC-measured heat release (ΔH_{DSC}) compared with IR-measured heat transfer (ΔH_{IR}) in experiments **1** to **5**. (**G**) Summary of key factors influencing the heat-transfer process. (**H**) Optical and IR images showing the physical and temperature changes of D-**3** solution during acid-triggered heat release, demonstrating sufficient energy output to induce water boiling in experiment **2**.

In this experiment, the Dewar isomer, dissolved in water (Fig. 4B), reverts to its pyrimidone form upon triggering, releasing heat to the aqueous solution. To promote the reversion, we used an acid catalyst—i.e., hydrochloric acid (HCl)—which efficiently accelerates the back isomerization (Fig. 4C). This strategy was only made possible by the deliberate incorporation of a nitrogen atom at the bridgehead position of the Dewar isomer (fig. S47). Computations indicate that protonation of the nitrogen lowers $\Delta H^{\ddagger}_{cal}$ by twofold, thereby enabling spontaneous reversion at room temperature. After heat release, the protonated product can be neutralized to regenerate the original pyrimidone, followed by photo-recharging to form the Dewar isomer. The cyclability of the process was confirmed experimentally (fig. S48).

We note that the use of homogeneous acid catalysts (e.g., HCl) necessitates a neutralization step, which leads to salt accumulation that reduces the total energy density. In a practical device configuration, a heterogeneous catalytic process would be preferable because it would eliminate the need for post–energy release treatment (*30*). Efforts to develop heterogeneous catalysts to facilitate the electrocyclic ring opening of Dewar pyrimidones represent a promising and important avenue for our future work.

To quantify the heat transfer from D-**3** to water activated by a catalyst (i.e., HCl), we devised experiment **1**, in which the solution temperature was monitored by infrared (IR) thermal imaging (Fig. 4, B and D). We note that deviations are expected between DSC-measured values (ΔH_{DSC}) and macroscopic IR measurements of heat transferred to a medium (ΔH_{IR}). This is because DSC measurements are performed on neat samples (<5 mg) under thermally insulated conditions with dynamic heating, whereas acid-catalyzed heat release from D-**3** (>50 mg) occurs in a heat-transfer medium, accompanied by heat dissipation to the surroundings.

In experiment **1**, upon addition of HCl (0.5 mmol, 2 M) under ambient conditions, D-**3** (51 mg in 0.50 ml of water) rapidly reverted within 1.8 s, producing a temperature increase (ΔT_{IR}) of 40°C (Fig. 4E). This corresponds to a heat transfer of 85 J (ΔH_{IR}) to the aqueous medium (Fig. 4F and table S7), which is comparable to ΔH_{DSC} (85 J).

Building on the benchmark experiment **1**, we calculated the amount of D-**3** needed to boil water. Raising 0.50 ml of water from room temperature to its boiling point ($\Delta T \approx 75$°C) requires ~165 J of thermal energy, corresponding to 100 mg of D-**3** (table S7, entry "calc"). However, boiling of the aqueous solution requires additional energy to overcome the enthalpy of vaporization [2.3 kJ g^{-1} (*92*)]. Therefore, the concentration of D-**3** was slightly increased by using 107 mg in 0.46 ml of water.

In experiment **2**, we demonstrated that addition of HCl (1.0 mmol, 4.5 M) to D-**3** solution raised the solution temperature to 100°C and induced boiling within 1 s (movie S1). IR thermal imaging measured a ΔT_{IR} of 76°C, corresponding to a ΔH_{IR} of 153 J transferred to the

aqueous solution (Fig. 4, E and F), whereas 107 mg of D-***3*** is expected to release 176 J (ΔH_{DSC}). We therefore attribute the energy difference ($\Delta\Delta H = 23$ J) to the boiling process, an amount sufficient to vaporize ~10 µl (2.2%) of water. After reaching the initial peak, the water temperature decreased gradually (movie S1).

We note that additional exotherm from the protonation process contributes to the measured heat transfer (ΔH_{IR}) in experiments **1** and **2**. To quantify the exotherm, we performed a control experiment ***3***, where P-***3*** (106 mg in 0.46 ml of water) was protonated to increase the temperature by only 7°C, corresponding to 14 J of heat transfer (Fig. 4, E and F). This confirms that the substantial total heat transfer observed in experiments **1** and **2** primarily originates from the energy released from the reverse Dewar isomerization rather than from protonation.

Previously, quadricyclanes have been shown to release heat in highly controlled experiments using a thermally insulated vacuum chamber to minimize heat loss (*90*). In such experiments, a solution of quadricyclane (1.5 M) in toluene was continuously flowed (5 ml h^{-1}) through a catalytic channel consisting of cobalt phthalocyanine on an alumina surface. The reversion induced a maximum temperature increase of 63°C after 2.5 min. Under these conditions, ~70 mg of quadricyclane transferred 27 J of thermal energy to 0.21 ml of solution, corresponding to a normalized transferred energy of 0.38 MJ kg^{-1}, which is comparable to the energy density measured by DSC (0.40 MJ kg^{-1}). In our work, D-***3*** with a substantially higher energy density (1.65 MJ kg^{-1}) enables rapid heating and boiling of water under ambient conditions at comparable or lower concentrations.

Beyond quadricyclanes catalyzed by metal complexes, we also performed acid-catalyzed heat-release experiments using other representative MOST compounds, namely diazetidine and *cis*-azobenzene (Fig. 4D, experiments **4** and **5**). Because both diazetidine and *cis*-azobenzene are poorly soluble in water, benzene was used as the heat-transfer medium, and trifluoroacetic acid (1.0 mmol, 4.5 M) was used as the catalyst. Under comparable mass loadings (~106 mg), D-***3*** transferred substantially more heat (153 J) to the medium compared with diazetidine (14 J) and *cis*-azobenzene (11 J) (Fig. 4F). This trend is consistent with the higher gravimetric energy density of D-***3*** (1.65 MJ kg^{-1}) compared with those of diazetidine (0.32 MJ kg^{-1}) and *cis*-azobenzene (0.23 MJ kg^{-1}) (table S7). The heat-release processes and the NMR analysis confirming complete reversions are illustrated in detail in movies S2 to S5 and figs. S49 to S56.

We note that benzene has a lower heat capacity (1.7 J g^{-1} K^{-1}) than water (4.2 J g^{-1} K^{-1}) (*93*, *94*). Therefore, diazetidine and *cis*-azobenzene reach maximum temperatures of 42° and 34°C, respectively, despite transferring only 14 J and 11 J of energy to the medium (Fig. 4, E and F, experiments **4** and **5**). On the basis of these results, we conclude that the maximum attainable temperature of the medium is governed by three parameters: (i) the gravimetric energy density of the MOST compound, (ii) the heat capacity of the medium, and (iii) the mass of the MOST compound dissolved (Fig. 4G).

Moreover, the difference between the released enthalpy measured by DSC and the heat transferred to the medium ($\Delta\Delta H = \Delta H_{DSC} - \Delta H_{IR}$) is substantial for diazetidine and *cis*-azobenzene (Fig. 4F, experiments **4** and **5**), despite the absence of boiling. Specifically, only 42 and 48% of the released energy was delivered to the medium for diazetidine and *cis*-azobenzene, respectively (table S7). These results suggest that, even under similar experimental conditions, the heat-transfer efficiency ($\Delta H_{IR}/\Delta H_{DSC}$) depends strongly on the reaction rate. For diazetidine, which is initially insoluble in benzene and slowly dissolves upon protonation (fig. S49), it takes 7.6 s to reach the maximum temperature during the heat release and transfer, thereby it is subject to greater heat loss to the surroundings (Fig. 4E). In the case of *cis*-azobenzene, despite its high solubility, the protonation and heat-release process appear to be slower (2.4 s) than those of Dewar pyrimidone, which similarly contributes to heat loss to the surroundings during heat release and transfer. Therefore, we propose that both (i) solubility and (ii) reaction rate are important factors influencing heat-transfer efficiency under ambient conditions (Fig. 4G).

Overall, we show that high–energy density Dewar pyrimidone (1.65 MJ kg^{-1}) can be efficiently catalyzed to release its stored heat and transfer it to an environmentally benign medium, such as water (Fig. 4H). Although this proof-of-concept experiment has not yet been optimized, it highlights the potential of this molecular fuel for practical heating applications. Future work will focus on integrating heterogeneous catalysts immobilized within the channel near a heat exchanger (Fig. 4A), allowing the Dewar solution to flow through and be activated in situ without the need for post–heat release treatment before recharging. The released heat can be extracted through a heat exchanger and delivered to a heat-transfer fluid (e.g., water) for heating applications.

Conclusions

In this work, we developed a pyrimidone-based MOST system guided by two key principles: (i) the incorporation of a highly strained, dearomatized aza-bicyclic scaffold to maximize stored energy and (ii) nitrogen incorporated at the reactive site to provide precise control over thermal release. Together, these features yielded a compact molecular architecture with an energy density of 1.65 MJ kg^{-1}. As a proof of concept, we demonstrated heat delivery sufficient to boil 0.46 ml (460 mg) of water using 107 mg of a MOST material. This result marks an important step in advancing MOST technologies from concepts to practical, scalable solutions for water heating, cooking, and surface defrosting in everyday settings.

Materials and methods are available in the supplementary materials.

REFERENCES AND NOTES

1. IRENA, IEA, REN21, "Renewable Energy Policies in a Time of Transition: Heating and Cooling" (2020); https://www.iea.org/reports/renewable-energy-policies-in-a-time-of-transition-heating-and-cooling.
2. International Energy Agency (IEA), Heating (2023); https://www.iea.org/energy-system/buildings/heating.
3. Alternative Fuels Data Center, Fuel Properties Comparison; https://afdc.energy.gov/fuels/properties.
4. R. Götz *et al.*, All-solid-state Li-ion batteries with commercially available electrolytes: A feasibility review. *InfoMat* **6**, e12627 (2024). doi: 10.1002/inf2.12627
5. M. U. Farid *et al.*, Technological advancements in water heating approaches for membrane distillation desalination process: From bulk to localized heating. *Desalination* **574**, 117235 (2024). doi: 10.1016/j.desal.2023.117235
6. G. R. Gossweiler *et al.*, Mechanochemically Active Soft Robots. *ACS Appl. Mater. Interfaces* **7**, 22431–22435 (2015). doi: 10.1021/acsami.5b06440; pmid: 26390078
7. Z. S. Kean *et al.*, Photomechanical actuation of ligand geometry in enantioselective catalysis. *Angew. Chem. Int. Ed.* **53**, 14508–14511 (2014). doi: 10.1002/anie.201407494; pmid: 25359436
8. A. M. Alfaraidi *et al.*, Reversible CO_2 Capture and On-Demand Release by an Acidity-Matched Organic Photoswitch. *J. Am. Chem. Soc.* **145**, 26720–26727 (2023). doi: 10.1021/jacs.3c08471; pmid: 38051161
9. P. Wójcik *et al.*, Photoswitching Molecules Functionalized with Optical Cycling Centers Provide a Novel Platform for Studying Chemical Transformations in Ultracold Molecules. *J. Phys. Chem. A* **129**, 1929–1940 (2025). doi: 10.1021/acs.jpca.4c06320; pmid: 39700511
10. A. Siiskonen, S. Vesamäki, A. Priimagi, Azobenzene protonation as a tool for temperature sensing. *Beilstein J. Org. Chem.* **21**, 1528–1534 (2025). doi: 10.3762/bjoc.21.115; pmid: 40761759
11. C. M. Tobin *et al.*, Reversible and size-controlled assembly of reflectin proteins using a charged azobenzene photoswitch. *Chem. Sci.* **15**, 13279–13289 (2024). doi: 10.1039/D4SC03299C; pmid: 39183923
12. T. Wachsmuth, R. Kluifhooft, M. Müller, L. Zeiß, M. Kathan, A molecular machine directs the synthesis of a catenane. *Science* **389**, 526–531 (2025). doi: 10.1126/science.adx5363; pmid: 40743339
13. L. Dong, Y. Feng, L. Wang, W. Feng, Azobenzene-based solar thermal fuels: Design, properties, and applications. *Chem. Soc. Rev.* **47**, 7339–7368 (2018). doi: 10.1039/C8CS00470F; pmid: 30168543
14. R. Losantos, D. Sampedro, Design and Tuning of Photoswitches for Solar Energy Storage. *Molecules* **26**, 3796 (2021). doi: 10.3390/molecules26133796; pmid: 34206445
15. Q. Qiu *et al.*, Photon Energy Storage in Strained Cyclic Hydrazones: Emerging Molecular Solar Thermal Energy Storage Compounds. *J. Am. Chem. Soc.* **144**, 12627–12631 (2022). doi: 10.1021/jacs.2c05384; pmid: 35801820

16. Z. Wang *et al.*, Evaluating Dihydroazulene/Vinylheptafulvene Photoswitches for Solar Energy Storage Applications. *ChemSusChem* **10**, 3049–3055 (2017). doi: 10.1002/cssc.201700679; pmid: 28644559
17. M. Brøndsted Nielsen, N. Ree, K. V. Mikkelsen, M. Cacciarini, Tuning the dihydroazulene – vinylheptafulvene couple for storage of solar energy. *Russ. Chem. Rev.* **89**, 573–586 (2020). doi: 10.1070/RCR4944
18. A. Lennartson, A. Lundin, K. Börjesson, V. Gray, K. Moth-Poulsen, Tuning the photochemical properties of the fulvalene-tetracarbonyl-diruthenium system. *Dalton Trans.* **45**, 8740–8744 (2016). doi: 10.1039/C6DT01343K; pmid: 27109432
19. K. Börjesson *et al.*, Exploring the potential of fulvalene dimetals as platforms for molecular solar thermal energy storage: Computations, syntheses, structures, kinetics, and catalysis. *Chemistry* **20**, 15587–15604 (2014). doi: 10.1002/chem.201404170; pmid: 25284044
20. Y. Kanai, V. Srinivasan, S. K. Meier, K. P. C. Vollhardt, J. C. Grossman, Mechanism of thermal reversal of the (fulvalene)tetracarbonyldiruthenium photoisomerization: Toward molecular solar-thermal energy storage. *Angew. Chem. Int. Ed.* **49**, 8926–8929 (2010). doi: 10.1002/anie.201002994; pmid: 20949567
21. R. R. Weber, C. N. Stindt, A. M. J. van der Harten, B. L. Feringa, Push-Pull Bis-Norbornadienes for Solar Thermal Energy Storage. *Chemistry* **30**, e202400482 (2024). doi: 10.1002/chem.202400482; pmid: 38519425
22. K. Jorner *et al.*, Unraveling factors leading to efficient norbornadiene–quadricyclane molecular solar-thermal energy storage systems. *J. Mater. Chem. A* **5**, 12369–12378 (2017). doi: 10.1039/C7TA04259K
23. R. Schulte, S. Afflerbach, T. Paululat, H. Ihmels, Bis- and Tris-norbornadienes with High Energy Densities for Efficient Molecular Solar Thermal Energy Storage. *Angew. Chem. Int. Ed.* **62**, e202309544 (2023). doi: 10.1002/anie.202309544; pmid: 37504899
24. L. Fei *et al.*, Two-way photoswitching norbornadiene derivatives for solar energy storage. *Chem. Sci.* **15**, 18179–18186 (2024). doi: 10.1039/D4SC04247F; pmid: 39421198
25. M. Mansø *et al.*, Molecular solar thermal energy storage in photoswitch oligomers increases energy densities and storage times. *Nat. Commun.* **9**, 1945 (2018). doi: 10.1038/s41467-018-04230-8; pmid: 29769524
26. X. An, Y. Xie, Enthalpy of isomerization of quadricyclane to norbornadiene. *Thermochim. Acta* **220**, 17–25 (1993). doi: 10.1016/0040-6031(93)80451-F
27. A. U. Petersen *et al.*, Solar Energy Storage by Molecular Norbornadiene-Quadricyclane Photoswitches: Polymer Film Devices. *Adv. Sci.* **6**, 1900367 (2019). doi: 10.1002/advs.201900367; pmid: 31380172
28. M. Quant *et al.*, Low Molecular Weight Norbornadiene Derivatives for Molecular Solar-Thermal Energy Storage. *Chemistry* **22**, 13265–13274 (2016). doi: 10.1002/chem.201602530; pmid: 27492997
29. M. Quant *et al.*, Synthesis, characterization and computational evaluation of bicyclooctadienes towards molecular solar thermal energy storage. *Chem. Sci.* **13**, 834–841 (2021). doi: 10.1039/D1SC05791J; pmid: 35173948
30. Z. Hussain *et al.*, Heterogeneously Catalyzed Energy Release in Azaborinine-based Molecular Solar Thermal Systems. *Top. Catal.* **68**, 1883–1891 (2025). doi: 10.1007/s11244-025-02089-w
31. K. Edel *et al.*, The Dewar Isomer of 1,2-Dihydro-1,2-azaborinines: Isolation, Fragmentation, and Energy Storage. *Angew. Chem. Int. Ed.* **57**, 5296–5300 (2018). doi: 10.1002/anie.201712683; pmid: 29457683
32. S. Chakraborty *et al.*, Curved anthracenes for visible-light photon energy storage via Dewar isomerization. *Chem* **11**, 102660 (2025). doi: 10.1016/j.chempr.2025.102660; pmid: 40857469
33. S. Helmy *et al.*, Photoswitching using visible light: A new class of organic photochromic molecules. *J. Am. Chem. Soc.* **136**, 8169–8172 (2014). doi: 10.1021/ja503016b; pmid: 24848124
34. J. Gemen *et al.*, Disequilibrating azobenzenes by visible-light sensitization under confinement. *Science* **381**, 1357–1363 (2023). doi: 10.1126/science.adh9059; pmid: 37733864
35. G. C. Thaggard *et al.*, Breaking the photoswitch speed limit. *Nat. Commun.* **14**, 7556 (2023). doi: 10.1038/s41467-023-43405-w; pmid: 37985777
36. J. Haimerl *et al.*, Shifting Gears: Photochromic Metal-Organic Frameworks with Stimulus-Adaptable Performance. *J. Am. Chem. Soc.* **147**, 19918–19930 (2025). doi: 10.1021/jacs.5c04466; pmid: 40442889
37. A. D. W. Kennedy, I. Sandler, J. Andréasson, J. Ho, J. E. Beves, Visible-Light Photoswitching by Azobenzazoles. *Chemistry* **26**, 1103–1110 (2020). doi: 10.1002/chem.201904309; pmid: 31729050
38. H. Qian, S. Pramanik, I. Aprahamian, Photochromic Hydrazone Switches with Extremely Long Thermal Half-Lives. *J. Am. Chem. Soc.* **139**, 9140–9143 (2017). doi: 10.1021/jacs.7b04993; pmid: 28644015
39. B. Shao, H. Fu, I. Aprahamian, A molecular anion pump. *Science* **385**, 544–549 (2024). doi: 10.1126/science.adp3506; pmid: 39088617
40. D. Kolarski, P. Steinbach, C. Bannwarth, K. Klaue, S. Hecht, Diaryltriazolium Photoswitch: Reaching a Millisecond Cycloreversion with High Stability and NIR Absorption. *Angew. Chem. Int. Ed.* **63**, e202318015 (2024). doi: 10.1002/ange.202318015; pmid: 38116882
41. J. Wu, L. Kreimendahl, J. L. Greenfield, Enhancing the Photoswitching Properties of *N*-Alkyl Imines. *J. Am. Chem. Soc.* **147**, 17549–17554 (2025). doi: 10.1021/jacs.5c02404; pmid: 40374166
42. M. Purdy, A. Y. Wang, M. C. Drummer, D. G. Nocera, R. Y. Liu, Reversible fluorenol photobases that perform CO_2 capture and concentration from ambient air. *Nat. Chem.* **17**, 1680–1687 (2025). doi: 10.1038/s41557-025-01901-0; pmid: 40804536
43. K. Kuntze *et al.*, A visible-light-driven molecular motor based on barbituric acid. *Chem. Sci.* **14**, 8458–8465 (2023). doi: 10.1039/D3SC03090C; pmid: 37592992
44. J. Calbo *et al.*, Tuning Azoheteroarene Photoswitch Performance through Heteroaryl Design. *J. Am. Chem. Soc.* **139**, 1261–1274 (2017). doi: 10.1021/jacs.6b11626; pmid: 28009517
45. N. J. Oldenhuis *et al.*, Photoswitchable Sol-Gel Transitions and Catalysis Mediated by Polymer Networks with Coumarin-Decorated Cu_{24} L_{24} Metal-Organic Cages as Junctions. *Angew. Chem. Int. Ed.* **59**, 2784–2792 (2020). doi: 10.1002/anie.201913297; pmid: 31742840
46. J. Wang *et al.*, Altering the Properties of Spiropyran Switches Using Coordination Cages with Different Symmetries. *J. Am. Chem. Soc.* **144**, 21244–21254 (2022). doi: 10.1021/jacs.2c08901; pmid: 36377832
47. H. P. Q. Nguyen, A. Mukherjee, J. Usuba, J. Wan, G. G. D. Han, Large and long-term photon energy storage in diazetidines *via* [2+2] photocycloaddition. *Chem. Sci.* **15**, 18846–18854 (2024). doi: 10.1039/D4SC05374E; pmid: 39483249
48. M. A. Gerkman *et al.*, Arylazopyrazoles for Long-Term Thermal Energy Storage and Optically Triggered Heat Release below 0 °C. *J. Am. Chem. Soc.* **142**, 8688–8695 (2020). doi: 10.1021/jacs.0c00374; pmid: 32319773
49. Y. Shi, M. A. Gerkman, Q. Qiu, S. Zhang, G. G. D. Han, Sunlight-activated phase change materials for controlled heat storage and triggered release. *J. Mater. Chem. A* **9**, 9798–9808 (2021). doi: 10.1039/D1TA01007G
50. S. Chakraborty *et al.*, Self-activated energy release cascade from anthracene-based solid-state molecular solar thermal energy storage systems. *Chem* **10**, 3309–3322 (2024). doi: 10.1016/j.chempr.2024.06.033; pmid: 39830017
51. A. Giménez-Gómez *et al.*, State-of-the-art and challenges towards a Molecular Solar Thermal (MOST) energy storage device. *React. Chem. Eng.* **9**, 1629–1640 (2024). doi: 10.1039/D4RE00131A
52. H. F. Bettinger, O. Hauler, Ring opening of 2-aza-3-borabicyclo[2.2.0]hex-5-ene, the Dewar form of 1,2-dihydro-1,2-azaborine: Stepwise versus concerted mechanisms. *Beilstein J. Org. Chem.* **9**, 761–766 (2013). doi: 10.3762/bjoc.9.86; pmid: 23766788
53. P. von Ragué Schleyer, M. Manoharan, H. Jiao, F. Stahl, The acenes: Is there a relationship between aromatic stabilization and reactivity? *Org. Lett.* **3**, 3643–3646 (2001). doi: 10.1021/ol016553b; pmid: 11700102
54. A. T. Balaban, Pv. Schleyer, H. S. Rzepa, Crocker, not Armit and Robinson, begat the six aromatic electrons. *Chem. Rev.* **105**, 3436–3447 (2005). doi: 10.1021/cr0300946; pmid: 16218557
55. US Food and Drug Administration, Ultraviolet (UV) Radiation (2020); https://www.fda.gov/radiation-emitting-products/tanning/ultraviolet-uv-radiation#UVCrisks.
56. F. Hemauer, H.-P. Steinrück, C. Papp, The Norbornadiene/Quadricyclane Pair as Molecular Solar Thermal Energy Storage System: Surface Science Investigations. *Chemphyschem* **25**, e202300806 (2024). doi: 10.1002/cphc.202300806; pmid: 38375756
57. R. C. Richter *et al.*, Facile Energy Release from Substituted Dewar Isomers of 1,2-Dihydro-1,2-Azaborinines Catalyzed by Coinage Metal Lewis Acids. *Angew. Chem. Int. Ed.* **63**, e202405818 (2024). doi: 10.1002/anie.202405818; pmid: 38665012
58. G. C. Thaggard, N. B. Shustova, COFs in the Game: Harvest Water to Sustain. *ACS Cent. Sci.* **11**, 653–655 (2025). doi: 10.1021/acscentsci.5c00357; pmid: 40463328
59. A. M. Alfaraidi *et al.*, An Extremely Stable and Soluble NH_2-Substituted Anthraquinone Electrolyte for Aqueous Redox Flow Batteries. *ACS Appl. Energy Mater.* **6**, 12259–12266 (2023). doi: 10.1021/acsaem.3c01943
60. P. Lentes *et al.*, Photoswitching of Diazocines in Aqueous Media. *J. Org. Chem.* **86**, 4355–4360 (2021). doi: 10.1021/acs.joc.1c00065; pmid: 33606536
61. P. Commins, M. A. Garcia-Garibay, Photochromic molecular gyroscope with solid state rotational states determined by an azobenzene bridge. *J. Org. Chem.* **79**, 1611–1619 (2014). doi: 10.1021/jo402516n; pmid: 24428572
62. N. B. Shustova, Anthracene-based energy storage. *Joule* **8**, 2957–2959 (2024). doi: 10.1016/j.joule.2024.10.015
63. J. Yamamoto, P. Plaza, K. Brettel, Repair of (6-4) Lesions in DNA by (6-4) Photolyase: 20 Years of Quest for the Photoreaction Mechanism. *Photochem. Photobiol.* **93**, 51–66 (2017). doi: 10.1111/php.12696; pmid: 27992654
64. D. Perdiz *et al.*, Distribution and repair of bipyrimidine photoproducts in solar UV-irradiated mammalian cells. *J. Biol. Chem.* **275**, 26732–26742 (2000). doi: 10.1016/S0021-9258(19)61437-7; pmid: 10827179
65. T. Douki, A. Reynaud-Angelin, J. Cadet, E. Sage, Bipyrimidine photoproducts rather than oxidative lesions are the main type of DNA damage involved in the genotoxic effect of solar UVA radiation. *Biochemistry* **42**, 9221–9226 (2003). doi: 10.1021/bi034593c; pmid: 12885257
66. R. C. De Selms, W. R. Schleigh, Heterocyclodieneone photochemistry I. Photo-2-pyridone (2-aza-3-oxobicyclo[2.2.0]hex-5-ene). *Tetrahedron Lett.* **13**, 3563–3566 (1972). doi: 10.1016/S0040-4039(01)94100-0

67. W. A. Ayer, R. Hayatsu, P. de Mayo, S. T. Reid, J. B. Stothers, The photodimers of α-pyridones. *Tetrahedron Lett.* **2**, 648–653 (1961). doi: 10.1016/S0040-4039(01)91666-1
68. S. Hirokami, T. Takahashi, M. Nagata, T. Yamazaki, Rearrangements of Dewar 4-pyrimidinones and 4-methoxy-2-azetidinones. Reactions through azetidinyl and acyl cations. *J. Org. Chem.* **52**, 2455–2468 (1987). doi: 10.1021/jo00388a022
69. S. Hirokami, A. Murao, H. Kakuda, H. Shinoda, Y. Koga, X-ray Crystal Structures and ab Initio Calculations on the Photochemically Formed Dewar Isomers of the 4(3*H*)-Pyrimidinone Derivatives. *J. Org. Chem.* **62**, 2711–2719 (1997). doi: 10.1021/jo962103z; pmid: 11671629
70. T. Nishio, A. Kato, C. Kashima, Y. Omote, Photochemical electrocyclization of 1,4,6-trisubstituted pyrimidin-2-ones to 2-oxo-1,3-diazabicyclo[2.2.0]hex-5-enes. *J. Chem. Soc. Perkin Trans. 1* **1980**, 607–610 (1980). doi: 10.1039/p19800000607
71. J. S. Taylor, D. S. Garrett, M. P. Cohrs, Solution-state structure of the Dewar pyrimidinone photoproduct of thymidylyl-(3′.fwdarw. 5′)-thymidine. *Biochemistry* **27**, 7206–7215 (1988). doi: 10.1021/bi00419a007; pmid: 3207670
72. S. A. Smith, Q. Cheng, G. Hill, D. H. Magers, Conventional strain energies of 1,2-dihydroazete, 2,3-dihydroazete, 1,2-dihydrophosphete, and 2,3-dihydrophosphete. *Struct. Chem.* **24**, 1681–1691 (2013). doi: 10.1007/s11224-012-0186-9
73. G. W. Breton, K. L. Martin, Are 1,2-dihydrodiazetes aromatic? An experimental and computational investigation. *J. Org. Chem.* **67**, 6699–6704 (2002). doi: 10.1021/jo026082m; pmid: 12227799
74. L. E. Gusel'nikov, V. G. Avakyan, S. L. Guselnikov, Hetero-π-systems from 2 + 2 cycloreversion, part 2. [1]Ab initio thermochemical study of heterocyclobutanes 2 + 2 cycloreversion to form heteroethenes $H_2C{=}X$ (X=NH, O, SiH_2, PH, S). *Heteroatom Chem.* **18**, 704–720 (2007). doi: 10.1002/hc.20377
75. K. B. Wiberg, G. Bonneville, R. Dempsey, Strain Energies of Small Ring Alkenes. *Isr. J. Chem.* **23**, 85–92 (1983). doi: 10.1002/ijch.198300011
76. L. Lapinski, M. J. Nowak, A. Les, L. Adamowicz, Ab Initio Calculations of IR Spectra in Identification of Products of Matrix Isolation Photochemistry: Dewar Form of 4(3H)-Pyrimidinone. *J. Am. Chem. Soc.* **116**, 1461–1467 (1994). doi: 10.1021/ja00083a035
77. M. A. El-Sayed, Triplet state. Its radiative and nonradiative properties. *Acc. Chem. Res.* **1**, 8–16 (1968). doi: 10.1021/ar50001a002
78. ASTM International, "Standard Tables for Reference Solar Spectral Irradiances: Direct Normal and Hemispherical on 37° Tilted Surface" (ASTM G173-23, 2023); https://store.astm.org/g0173-23.html.
79. University of Wisconsin–Green Bay, "Heating Fuel Life-cycle Assessment" (Pellet Fuels Institute, Final Report, 2007); https://www.pelletheat.org/assets/docs/industry-data/final-pfi-study.pdf.
80. N. Jungbluth, P. Wenzel, C. Meili, "Life cycle inventories of oil heating systems: Final report" (ESU-services Ltd., 2018); https://esu-services.ch/fileadmin/download/publicLCI/jungbluth-2018_LCI_of_oil_heating_systems.pdf.
81. S. M. Biebl, R. C. Richter, M. Ströbele, I. Fleischer, H. F. Bettinger, High energy density dihydroazaborinine dyads and triad for molecular solar thermal energy storage. *Chem. Sci.* **16**, 15231–15238 (2025). doi: 10.1039/D5SC03159A; pmid: 40727839
82. G. A. Kukier, A. Turlik, X.-S. Xue, K. N. Houk, Violations. How Nature Circumvents the Woodward–Hoffmann Rules and Promotes the Forbidden Conrotatory 4*n* + 2 Electron Electrocyclization of Prinzbach's Vinylogous Sesquifulvalene. *J. Am. Chem. Soc.* **143**, 21694–21704 (2021). doi: 10.1021/jacs.1c11058; pmid: 34911295
83. H. M. Frey, B. M. Pope, R. F. Skinner, Thermal isomerization of cyclobutenes. Part 10.—3,3-Dimethylcyclobutene and 1,3,3-trimethylcyclobutene. *Trans. Faraday Soc.* **63**, 1166–1170 (1967). doi: 10.1039/TF9676301166
84. P. Nava, Y. Carissan, On the ring-opening of substituted cyclobutene to benzocyclobutene: Analysis of π delocalization, hyperconjugation, and ring strain. *Phys. Chem. Chem. Phys.* **16**, 16196–16203 (2014). doi: 10.1039/C4CP01695E; pmid: 24968824
85. J. Kruszewski, T. M. Krygowski, Definition of aromaticity basing on the harmonic oscillator model. *Tetrahedron Lett.* **13**, 3839–3842 (1972). doi: 10.1016/S0040-4039(01)94175-9
86. T. M. Krygowski, Crystallographic studies of inter- and intramolecular interactions reflected in aromatic character of. pi.-electron systems. *J. Chem. Inf. Comput. Sci.* **33**, 70–78 (1993). doi: 10.1021/ci00011a011
87. M. G. Evans, M. Polanyi, Inertia and driving force of chemical reactions. *Trans. Faraday Soc.* **34**, 11–24 (1938). doi: 10.1039/tf9383400011
88. J. N. Bronsted, Acid and Basic Catalysis. *Chem. Rev.* **5**, 231–338 (1928). doi: 10.1021/cr60019a001
89. R. P. Bell, The theory of reactions involving proton transfers. *Proc. A* **154**, 414–429 (1997). doi: 10.1098/rspa.1936.0060
90. Z. Wang *et al.*, Macroscopic heat release in a molecular solar thermal energy storage system. *Energy Environ. Sci.* **12**, 187–193 (2019). doi: 10.1039/C8EE01011K
91. K. Moth-Poulsen *et al.*, Molecular solar thermal (MOST) energy storage and release system. *Energy Environ. Sci.* **5**, 8534–8537 (2012). doi: 10.1039/c2ee22426g
92. D. R. Lide Ed., *CRC Handbook of Chemistry and Physics* (CRC Press, ed. 84, 2004).
93. N. H. Almousa *et al.*, Paraffin Wax [As a Phase Changing Material (PCM)] Based Composites Containing Multi-Walled Carbon Nanotubes for Thermal Energy Storage (TES) Development. *Crystals* **11**, 951 (2021). doi: 10.3390/cryst11080951
94. J. P. E. Grolier, G. Roux-Desgranges, M. Berkane, E. Jiménez, E. Wilhelm, Heat capacities and densities of mixtures of very polar substances 2. Mixtures containing *N*, *N*-dimethylformamide. *J. Chem. Thermodyn.* **25**, 41–50 (1993). doi: 10.1006/jcht.1993.1005
95. H. Chen *et al.*, Water-Soluble Azobenzene-Based Solar Thermal Fuels with Improved Long-Term Energy Storage and Energy Density. *ACS Appl. Mater. Interfaces* **16**, 66837–66845 (2024). doi: 10.1021/acsami.3c12264; pmid: 37944917
96. R. J. Corruccini, E. C. Gilbert, The Heat of Combustion of *cis*- and *trans*-Azobenzene. *J. Am. Chem. Soc.* **61**, 2925–2927 (1939). doi: 10.1021/ja01265a100
97. A. Gonzalez *et al.*, Photocontrolled Energy Storage in Azobispyrazoles with Exceptionally Large Light Penetration Depths. *J. Am. Chem. Soc.* **144**, 19430–19436 (2022). doi: 10.1021/jacs.2c07537; pmid: 36222796
98. G. D. Han *et al.*, Photon energy storage materials with high energy densities based on diacetylene–azobenzene derivatives. *J. Mater. Chem. A* **4**, 16157–16165 (2016). doi: 10.1039/C6TA07086H
99. M. A. Morikawa, Y. Yamanaka, J. K. Ho Hui, N. Kimizuka, Photoliquefaction and phase transition of *m*-bisazobenzenes give molecular solar thermal fuels with a high energy density. *RSC Adv.* **13**, 24031–24037 (2023). doi: 10.1039/D3RA04595A; pmid: 37577092
100. Q. Qiu, M. A. Gerkman, Y. Shi, G. G. D. Han, Design of phase-transition molecular solar thermal energy storage compounds: Compact molecules with high energy densities. *Chem. Commun.* **57**, 9458–9461 (2021). doi: 10.1039/D1CC03742K; pmid: 34528978
101. D. Schatz, C. Averdunk, R. Fritzius, H. A. Wegner, An Azobenzene-Based Liquid Molecular Solar Thermal (MOST) Storage System-Energy Carrier and Solvent. *Small* **21**, e2502938 (2025). doi: 10.1002/smll.202502938; pmid: 40457655
102. S. Sun *et al.*, Photoswitches with different numbers of azo chromophores for molecular solar thermal storage. *Soft Matter* **18**, 8840–8849 (2022). doi: 10.1039/D2SM01073A; pmid: 36373235
103. W. Yang *et al.*, Efficient cycling utilization of solar-thermal energy for thermochromic displays with controllable heat output. *J. Mater. Chem. A* **7**, 97–106 (2019). doi: 10.1039/C8TA05333B
104. N. Baggi *et al.*, Exploring *ortho*-dianthrylbenzenes for molecular solar thermal energy storage. *J. Mater. Chem. A* **12**, 26457–26464 (2024). doi: 10.1039/D4TA03879G; pmid: 39219708
105. T. Nishiuchi, S. Y. Uno, Y. Hirao, T. Kubo, Intramolecular Interaction, Photoisomerization, and Mechanical C–C Bond Dissociation of 1,2-Di(9-anthryl)benzene and Its Photoisomer: A Fundamental Moiety of Anthracene-Based π-Cluster Molecules. *J. Org. Chem.* **81**, 2106–2112 (2016). doi: 10.1021/acs.joc.6b00134; pmid: 26828776
106. H. P. Q. Nguyen *et al.*, Molecular Solar Thermal Energy Storage in Dewar Pyrimidone Beyond 1.6 MJ/kg, *Dryad* (2026). doi: 10.5061/dryad.rxwdbrvqg

ACKNOWLEDGMENTS

Funding: This study was supported by National Science Foundation (NSF) CAREER award DMR-2142887 (G.G.D.H.); a 2025 Marion Milligan Mason Award for Women in the Chemical Sciences (American Association for the Advancement of Science) (G.G.D.H.); Alfred P. Sloan Foundation FG-2022-18328 (G.G.D.H.); Camille and Henry Dreyfus Foundation TC-23-028 (G.G.D.H.); Brandeis MRSEC DMR-2011846 (G.G.D.H.); Research Corporation for Science Advancement Collaborative Innovation Award SA-SM3-2024-057b (G.G.D.H.); NSF CHE-215372 (K.N.H.); NSF Graduate Research Fellowship DGE-2034835 (A.J.M.); and the Gordon and Betty Moore Foundation through grant GBMF13626 to the University of California, Santa Barbara (G.G.D.H.). **Author contributions:** Conceptualization: G.G.D.H., K.N.H., H.P.Q.N.; Funding acquisition: G.G.D.H., K.N.H., K.E.S.; Investigation: H.P.Q.N., A.J.M., B.A.B., N.M.-W.W., Z.Y., Q.Z., Q.Q., N.K., D.B.B.; Methodology: H.P.Q.N., A.J.M.; Project administration: G.G.D.H.; Supervision: G.G.D.H., K.N.H.; Visualization: G.G.D.H., H.P.Q.N.; Writing – original draft: H.P.Q.N., B.A.B., N.M.-W.W.; Writing – review & editing: G.G.D.H., K.N.H., H.P.Q.N., B.A.B., A.J.M., Q.Z. **Competing interests:** The authors declare that they have no competing interests. **Data, code, and materials availability:** All data are available in the main text or the supplementary materials. Data underlying the plots have been deposited at Dryad (*106*).

SUPPLEMENTARY MATERIALS

science.org/doi/10.1126/science.aec6413
Materials and Methods; Supplementary Text; Figs. S1 to S56; Tables S1 to S7; References (*107*–*145*); Movies S1 to S5

Submitted 30 September 2025; accepted 27 January 2026; published online 12 February 2026
10.1126/science.aec6413

Molecular solar thermal energy storage in Dewar pyrimidone beyond 1.6 megajoules per kilogram

Han P. Q. Nguyen, Alexander J. Maertens, Benjamin A. Baker, Nathan M.-W. Wu, Zihao Ye, Qingyang Zhou, Qianfeng Qiu, Navneet Kaur, David B. Berkinsky, Katherine E. Shulenberger, K. N. Houk, and Grace G. D. Han

Science **392** (6796), eaec6413. DOI: 10.1126/science.aec6413

Editor's summary

Most fuels produce heat through combustion reactions that are hard to reverse. Photoswitches offer the opportunity to store light energy from the sun and then release heat in a sustainable cycle; however, they tend to release comparatively little heat. Nguyen *et al*. now report a pyrimidone compound that isomerizes under ultraviolet irradiation to form a highly strained bond between a nitrogen and the diametrically opposite carbon. Upon treatment with acid, that bond breaks to release more than a megajoule per kilogram of the compound, enough to rapidly boil water from a solution. —Jake S. Yeston